Journal of the American College of Cardiology
© 2003 by the American College of Cardiology Foundation
Published by Elsevier Inc.

Vol. 41, No. 10, 2003
ISSN 0735-1097/03/$30.00
doi:10.1016/S0735-1097(03)00307-3

Assessment of Right Ventricular Perfusion After Right Coronary Artery Occlusion by Myocardial Contrast Echocardiography

Hisashi Masugata, MD,* Norihiro Fujita, MD,* Isao Kondo, MD,* Barry Peters, MD,† Koji Ohmori, MD,* Katsufumi Mizushige, MD, FACC,* Masakazu Kohno, MD,* Anthony N. DeMaria, MD, MACC†

Kita-gun, Japan; and San Diego, California

OBJECTIVES The purpose of this study was to examine the ability of myocardial contrast echocardiography (MCE) to assess right ventricular (RV) perfusion.

BACKGROUND Although MCE can readily assess left ventricular perfusion abnormalities, there are no data regarding the ability to assess RV perfusion abnormalities.

METHODS The right coronary artery (RCA) was occluded in 10 open-chest dogs. Myocardial contrast echocardiography was performed with 0.27 g/min Levovist infusion by harmonic power Doppler with electrocardiographically gated intermittent triggered imaging at pulsing intervals ranging from 1:1 to 1:20 at baseline and 90 min after RCA occlusion. Video-intensity of the RV wall was plotted against pulsing intervals and was fitted to an exponential function: $y = A(1\text{-}\exp^{-bt})$, where A is the plateau video-intensity and b is the rate of video-intensity rise. Myocardial contrast echocardiography and microsphere-derived myocardial blood flow (MBF) measurements were performed at baseline and 90 min after RCA occlusion.

RESULTS Because the severity of RV perfusion abnormalities assessed by MBF varied during RCA occlusion, diverse grades of patchy opacification defects were observed by MCE. The RV wall thickness decreased, and the RV dimension increased, after RCA occlusion in each dog. The correlation of occlusion to baseline MBF ratios in the RV wall was closer to the ratio of b ($r = 0.897$, $p = 0.0004$) than A ($r = 0.767$, $p = 0.0097$) and was the closest to the ratio of $A \times b$ ($r = 0.935$, $p < 0.0001$).

CONCLUSIONS The RCA occlusion is manifested by RV wall thinning and dilation as well as by perfusion abnormalities consisting of patchy opacification defects by MCE. Myocardial contrast echocardiography–derived refilling parameters can be applied to assess RV perfusion abnormalities produced by RCA occlusion. (J Am Coll Cardiol 2003;41:1823–30) © 2003 by the American College of Cardiology Foundation

Myocardial contrast echocardiography (MCE) has proven to be an effective method for visualizing left ventricular (LV) myocardial perfusion defects in the setting of coronary stenosis and obstructions in both experimental (1) and clinical (2) studies. Moreover, after microbubble destruction, parameters derived from plotting increasing video-intensity against time provide a method to quantify coronary blood flow by MCE (3) and thereby identify and quantify myocardial perfusion abnormalities. However, no data are available regarding the ability of MCE to identify and quantify perfusion abnormalities in the thinner right ventricular (RV) wall.

Myocardial contrast echocardiography assessment of RV perfusion would be of particular value in identifying RV infarction, which occurs in 30% of patients with LV inferior wall infarctions and is a strong predictor of arrhythmogenic and mechanical complications as well as in-hospital mortality (4). Although conventional echocardiography can assist in the diagnosis of RV infarction by detecting abnormal wall motion and/or dilation of the RV (5), it cannot delineate RV myocardial perfusion. Moreover, assessment of RV wall-motion abnormalities may be difficult with conventional echocardiography because the RV wall is thinner and exhibits less thickening and excursion than LV myocardium.

Levovist (Schering, Berlin, Germany) is an air-filled galactose microbubble coated with palmitic acid and has been used mainly to opacify the LV cavity in patients with suboptimal endocardial border definition by routine echocardiography (6). However, several recent studies have demonstrated the feasibility of applying this contrast agent to the assessment of myocardial perfusion by using harmonic power Doppler imaging (6,7). We hypothesized that MCE using Levovist can delineate and quantify RV myocardial perfusion abnormalities when power Doppler imaging is used. In this study, we sought to examine the abilities of MCE to assess RV myocardial perfusion abnormalities produced by right coronary artery (RCA) occlusion in open-chest dogs.

METHODS

Animal preparation. The study was approved by the Animal Research Committee of our institution. Ten mongrel dogs were anesthetized with 30 mg/kg sodium pentobarbi-

From the *Second Department of Internal Medicine, Kagawa Medical University, Kita-gun, Japan and †Cardiovascular Division, University of California at San Diego, San Diego, California. Dr. DeMaria has served as a grantee, member of the Scientific Advisory Board, or sponsored speaker for most ultrasound contrast agent manufacturers. Michael H. Picard, MD, acted as guest editor for this paper.

Manuscript received September 29, 2002; revised manuscript received December 25, 2002, accepted January 9, 2003.

Abbreviations and Acronyms

ECG = electrocardiogram/electrocardiographic
LCA = left coronary artery
LV = left ventricle/ventricular
MBF = myocardial blood flow
MCE = myocardial contrast echocardiography
RCA = right coronary artery
ROI = region of interest
RV = right ventricle/ventricular

tal, supplemented by 2 to 10 mg/kg/h intravenously to maintain a constant level of anesthesia. The dogs were intubated and ventilated. Both femoral veins and arteries were cannulated to inject the contrast agent, infuse saline to maintain hydration, measure hemodynamic parameters, and withdraw blood samples. The heart was exposed through a median sternotomy and suspended in a pericardial cradle. A fluid-filled catheter was introduced directly into the left atrium for injection of fluorescent microspheres. The proximal portion of the right coronary artery (RCA) was dissected free from the surrounding tissue to produce coronary occlusion.

MCE. Levovist of 2.5 g was diluted to a total volume of 8.5 ml (approximately 300 mg/ml). Contrast was produced by the continuous infusion of 0.27 g/min Levovist with a volumetric pump. A latex bag filled with degassed saline functioned as an acoustic interface between the heart and the transducer, which was positioned on the RV free wall to image the RCA perfusion territory. Imaging was performed with a broad band 1.6 to 3.2 MHz transducer (Harmonic Angio Mode, SONOS 5500; Philips Medical Systems, Andover, Massachusetts). Second harmonic color-coded power Doppler recording was performed with ultrasound transmitted at 1.6 MHz and received at 3.2 MHz in short-axis view at the LV outflow tract level during end-systolic electrocardiographic (ECG) triggering. A mechanical index of 1.3 was chosen, and focus was placed on the RV free wall to obtain optimal RV myocardial opacification for each experiment. Pulse repetition frequency was fixed at 6.9 kHz. The packet size, line density, overall gain, image depth, and wall filter were held constant for each experiment. The interval between the ECG triggers (pulsing interval) was increased from every heart beat (1:1) to every 2 (1:2), 4 (1:4), 6 (1:6), 8 (1:8), 10 (1:10), 15 (1:15), and 20 (1:20) cardiac cycles to allow incremental microbubble replenishment. End-systolic ECG gating was adjusted before contrast injection to minimize the clutter artifact due to cardiac motion, and the same triggering phase was used throughout each experiment.

Echocardiographic analysis. Myocardial contrast echocardiography images were analyzed off line as described previously (8,9). Images were acquired on S-VHS videotape before and after microbubble injection at each pulsing interval and were transferred to a Macintosh computer and aligned for background subtraction of myocardial video-intensity and measurement of RV wall thickness and dimension. Power Doppler images were converted to gray scale using National Institutes of Health Image 1.62 on an off-line computer. Color was ignored, and only myocardial luminance was assessed. Myocardial video-intensity was measured in gray scale units ranging from 0 to 255. Transmural regions of interest (ROIs) were selected which encompassed the central portion of the whole RV free wall in a short-axis image (Fig. 1). The size of the ROI was adjusted to include as much of the central RV free wall as could be imaged in each animal. Background-subtracted video-intensity was calculated for the ROI. Myocardial video-intensity versus pulsing interval plots were fitted to a 1-exponential function: $y = A(1-\exp^{-bt})$, where y is video-intensity, A is the plateau video-intensity, b is the rate of video-intensity rise (slope of the curve), and t is the pulsing interval (3). To assess RV function, the regional RV wall thickness and dimension were measured in the center of the RV free wall segment that was imaged (Fig. 1).

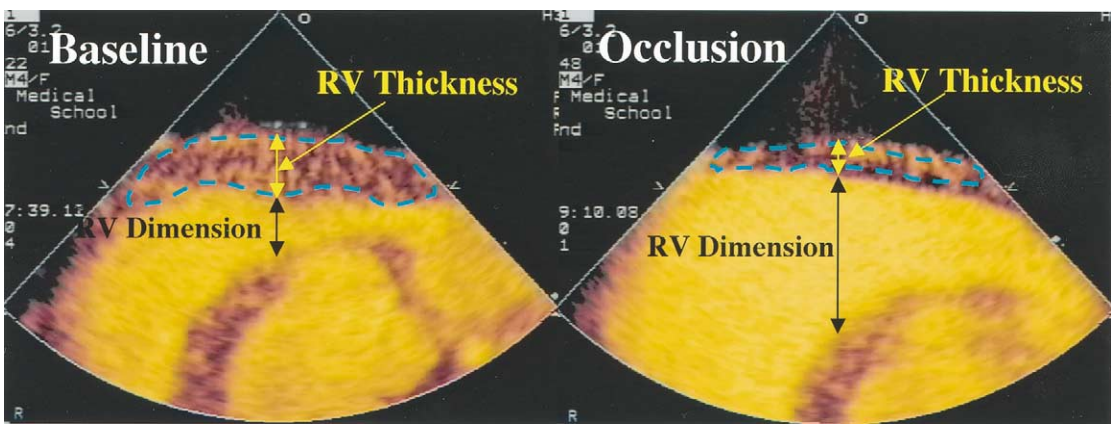

Figure 1. Myocardial contrast echocardiography images at baseline **(left)** and during coronary occlusion **(right)**. The blue line indicates the region of interest to measure video-intensity in the right ventricular (RV) wall for each image.

Myocardial blood flow measurement. Myocardial blood flow (MBF) was measured by injecting 5×10^6 10-μm fluorescent microspheres (Molecular Probes, Eugene, OR) directly into the left atrium. Reference blood samples were simultaneously withdrawn from the femoral artery with a constant rate pump at a withdrawal rate of 15 ml/min. After the animal was euthanized, the heart was explanted and sliced, and the cross-sectional slice of the RV corresponding to the echo short-axis image was cut into 12 wedge-shaped transmural tissue pieces. The tissue and the arterial reference sample were processed using a flow cytometer to count the microspheres.

Myocardial blood flow to each tissue piece was calculated from the equation $Qm = (Cm \times Qr)/Cr$, where Qm is the blood flow to the myocardial segment (ml/min), Cm is tissue count, Qr is rate of arterial sample withdrawal (ml/min), and Cr is the arterial reference sample count (10). Transmural MBF (ml/min/g) to 12 wedge-shaped pieces was calculated as the quotient of the flows to the individual pieces and the weight. The MBF to the risk area of an occluded RCA in the RV free wall was then determined by the wedge-shaped pieces corresponding to the risk area in the echo short-axis image.

In addition, the cross-sectional area of the RCA perfusion territory defined by blue dye injection [VIDE INFRA] was measured. The cross-sectional slice of the RV corresponding to the echo short-axis image was traced on transparencies. The RCA perfusion territory on the transparency was measured with planimetry in the NIH Image 1.62 software, and the percent of cross-sectional area of RCA perfusion territory was calculated in the RV free wall.

Experimental protocol. Baseline recording was obtained when hemodynamic stability was achieved (approximately 30 min after instrumentation). At that point, baseline MCE followed by MBF measurement was performed. Thereafter, the RCA was occluded by ligating the proximal portion of the RCA in a one-stage manner to produce RV perfusion abnormalities. At 90 min after RCA occlusion, when hemodynamics and regional wall-motion abnormalities were stable, a second MCE followed by MBF measurement was performed. At the end of the experiment, petroleum-based blue dye (SANFORD Corp., Bellwood, Illinois) was injected through the catheter introduced into the left atrium. This procedure allowed delineation of the RCA bed at the short-axis MCE imaging plane. The dogs were then euthanized, and the hearts were excised. The hearts were each cut into five short-axis slices, and the slice corresponding to the MCE imaging plane was processed for fluorescent microsphere analysis.

Statistical analysis. Data from all animals were expressed as mean ± SD. The Student paired *t* test was used to compare data between baseline and RCA occlusion. One-sample *t* test was used to assess percent changes in MBF and extent of risk area. Correlation between MCE and MBF data was performed by linear regression analysis. A p value of <0.05 was considered statistically significant.

RESULTS

Hemodynamic change. Systolic and diastolic blood pressure decreased at RCA occlusion (127 ± 20 and 86 ± 10 mm Hg) compared with baseline (138 ± 19 and 90 ± 11 mm Hg) ($p < 0.05$). The RV systolic pressure decreased (20 ± 6 vs. 16 ± 5 mm Hg) and RV end-diastolic pressure increased (3 ± 3 vs. 6 ± 4 mm Hg) by RCA occlusion ($p < 0.01$).

Visual identification of RV perfusion abnormalities by MCE. We assessed the RV perfusion abnormalities in each animal by visual analysis. Although RCA occlusion produced RV free-wall thinning and RV cavity dilation in all animals, the severity of the opacification defects varied markedly among animals. Figure 2 shows MCE images at varying pulsing intervals in an experiment in which a mild opacification defect (Mild) was produced and an experiment in which a severe defect (Severe) was produced by RCA occlusion. In the animal with a mild opacification defect, the intensity of RV wall opacification increased progressively with longer pulsing intervals during both baseline and RCA occlusion. A patchy opacification defect was felt to be present in the thinned RV wall during RCA occlusion. However, it was difficult to distinguish with certainty the decreased RV opacification during RCA occlusion from normal opacification at baseline by visual analysis because the decrease in RV opacification was small. In the animal with a severe opacification defect, the intensity of RV opacification also increased progressively with longer pulsing intervals at baseline and RCA occlusion. Although the opacification defect produced by RCA occlusion was also patchy, it was distinct from normal even during long pulsing intervals (1:4 to 1:20). However, the RCA risk area in the RV wall showed considerable opacification with prolongation of pulsing interval even in an animal with severe opacification defect.

Myocardial video-intensity in the RV wall and the parameters derived from exponential function. Figure 3 presents the background-subtracted video-intensity in the RV free wall during varying pulsing intervals obtained from the same two animals whose MCE images were shown in Figure 2. For the animal with a mild defect, the video-intensity in the RV wall progressively increased with prolongation of the pulsing interval during both baseline and RCA occlusion. The RV wall video-intensity during RCA occlusion was slightly less than baseline, as were *A* and *b* parameters during occlusion. For the animal with a severe opacification defect, RV wall video-intensity also increased with prolongation of the pulsing interval during both baseline and RCA occlusion. Although a decrease in the plateau video-intensity (*A* parameter) was also observed during occlusion from baseline, it was small. However, the rate of video-intensity rise (*b* parameter) during occlusion was markedly decreased compared with that during baseline.

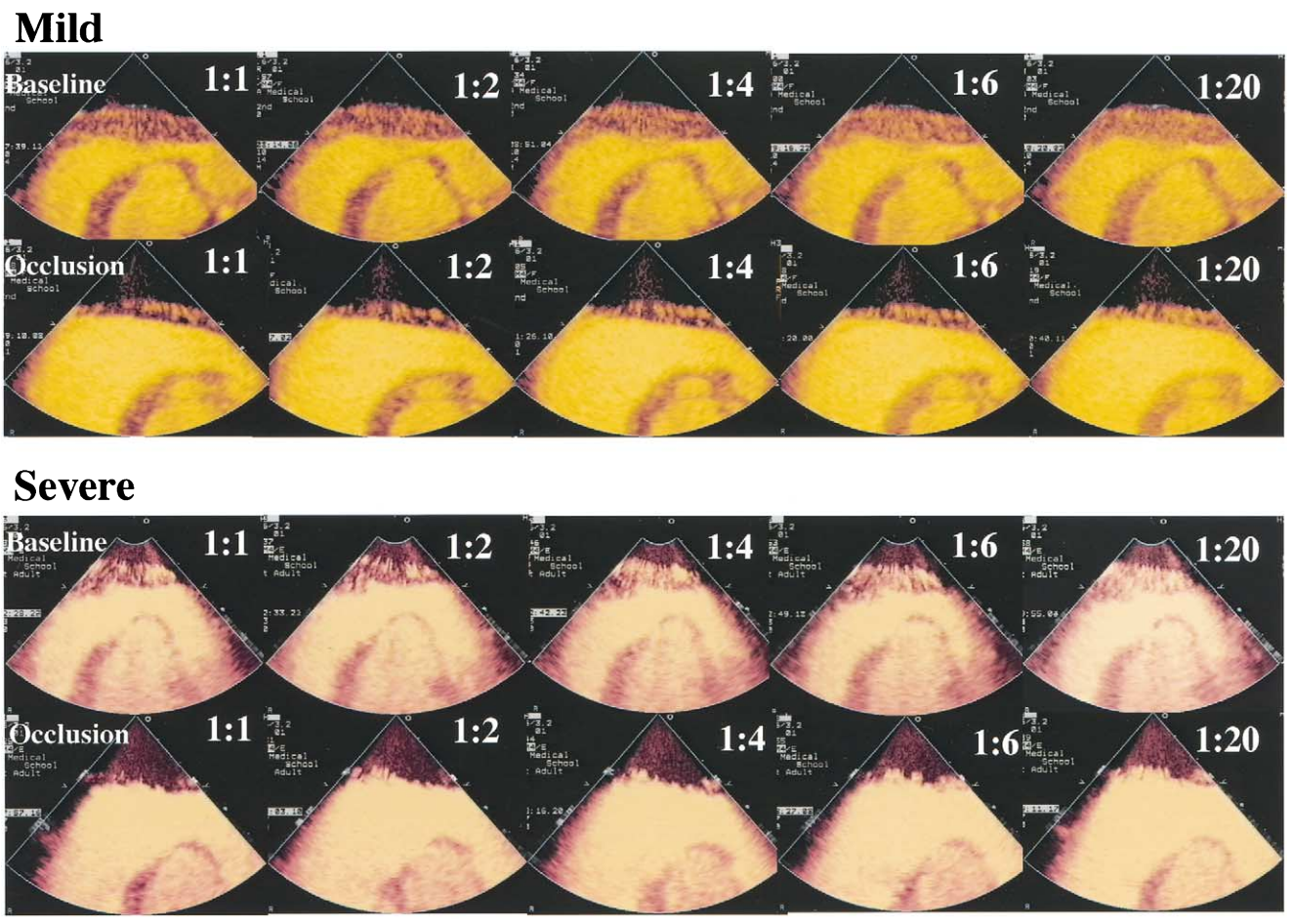

Figure 2. Myocardial contrast echocardiography images at varying pulsing intervals during baseline and right coronary artery occlusion from dogs with mild **(top)** and severe **(bottom)** opacification defects.

Risk area of an occluded RCA delineated by blue dye staining. Figure 4 shows the risk area of the RCA delineated by blue dye staining for the slice corresponding to the MCE imaging plane in the same animals as in Figures 2 and 3. Regions that were not stained by blue dye between arrows denote the RCA bed. Both animals showed risk areas located in the center of the RV free wall that were over 60% of the RV short-axis free-wall area. For the animal with a mild opacification defect, the risk area without blue dye was observed to be patchy, and the edge of the defect was indistinct rather than sharp. For the animal with a severe opacification defect, the risk area was homogeneous, and the edge of the defect was sharply delineated.

Changes in RV wall thickness, RV dimension, and MCE-derived parameters. Figure 5 (A and B) shows the changes in RV wall thickness and dimension measured where the ROIs were positioned for all 10 dogs. Right ventricular wall thickness decreased, and RV dimension increased, during RCA occlusion, compared with those at baseline in each dog. Figure 5 (C, D, and E) shows the changes in MCE-derived parameters produced by RCA occlusion in all 10 dogs. All parameters (*A*, *b*, and *Axb*) decreased during RCA occlusion, compared with those at baseline in each dog. The degree of change in all five parameters varied for each animal.

Extent of risk area and changes in microsphere-derived MBF. Figure 6 shows the values for risk area and changes in microsphere-derived MBF produced by RCA occlusion in all 10 dogs. The mean value for risk area expressed as a percentage of the RV short-axis free wall area was 75 ± 9% by blue dye staining (60% to 87%). Microsphere-derived MBF in the risk area decreased during RCA occlusion in each dog; however, the degrees of decrease varied for each animal. Thus, the percent of change in MBF produced by RCA occlusion was −45 ± 17% (−22% to −69%).

Correlation between MCE-derived parameters and MBF. Figure 7 (A, B, and C) shows the correlation between MCE-derived parameters and microsphere-derived MBF at baseline and RCA occlusion combined. Although there was significant intercept and deviation from the identity line, a good correlation was observed for all MCE-derived parameters (*A*: $r = 0.632$, $p = 0.0028$; *b*: $r = 0.789$, $p < 0.0001$; *Axb*: $r = 0.755$, $p = 0.0001$). In addition, we examined the correlation between the occlusion/baseline ratio of MCE-derived parameters and the similar ratio of RV structure and microsphere-derived MBF (D, E, and F in Fig. 7). Neither

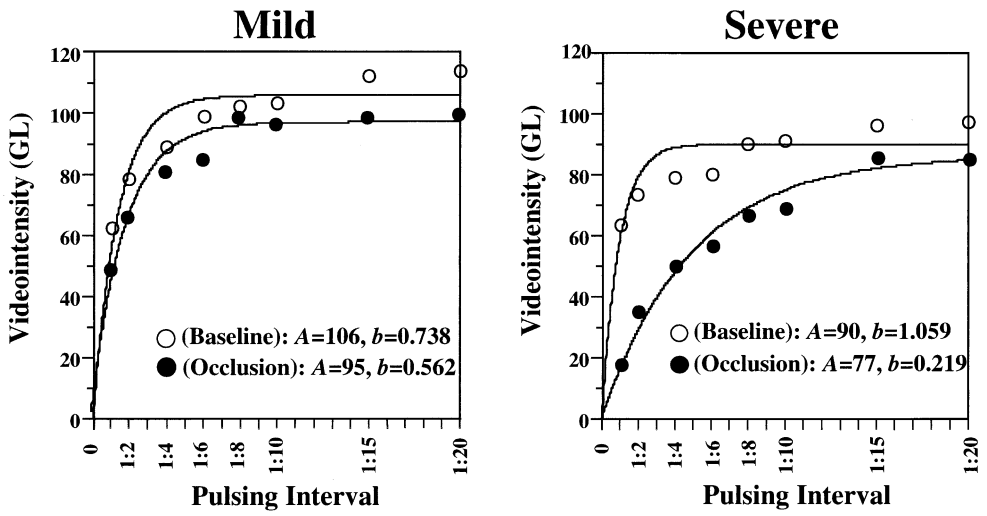

Figure 3. Plots of video-intensity (*y*-axis) versus pulsing interval (*x*-axis) from dogs shown in Figure 2, with mild **(left)** and severe **(right)** opacification defects.

the occlusion/baseline ratio of RV wall thickness ($r = 0.025$, $p = 0.94$) nor the dimension ($r = 0.206$, $p = 0.57$) correlated with the similar ratio of MBF. The occlusion/baseline ratio of the *A*, *b*, and *Axb* parameters correlated with that of MBF. The correlation of the *b* parameter ($r = 0.897$, $p = 0.0004$) was closer than that of the *A* parameter ($r = 0.767$, $p = 0.0097$), and the correlation of the *Axb* parameter ($r = 0.935$, $p < 0.0001$) was the closest among the three parameters.

DISCUSSION

The present study is the first quantitative assessment of the RV perfusion abnormalities delineated by MCE in the setting of RCA occlusion. Our findings indicate that: 1) ECG-triggered intermittent MCE enables visualization of patchy RV opacification defects produced by RCA occlusion even though the RV wall is thinned; 2) the magnitude of the opacification defect varies among animals; 3) although changes in RV wall thickness and dimension do not correlate with decrease in RV MBF produced by RCA occlusion, changes in MCE-derived parameters (*A*, *b*, *Axb*) correlate well with the decrease in RV MBF in the risk area; and 4) the correlation of *Axb* parameter with MBF is the closest among the three MCE parameters. These data indicate that although the defects are less homogeneous and of less severity than for the LV, visual and quantitative analysis of RV MCE detects abnormalities during RCA occlusion and may

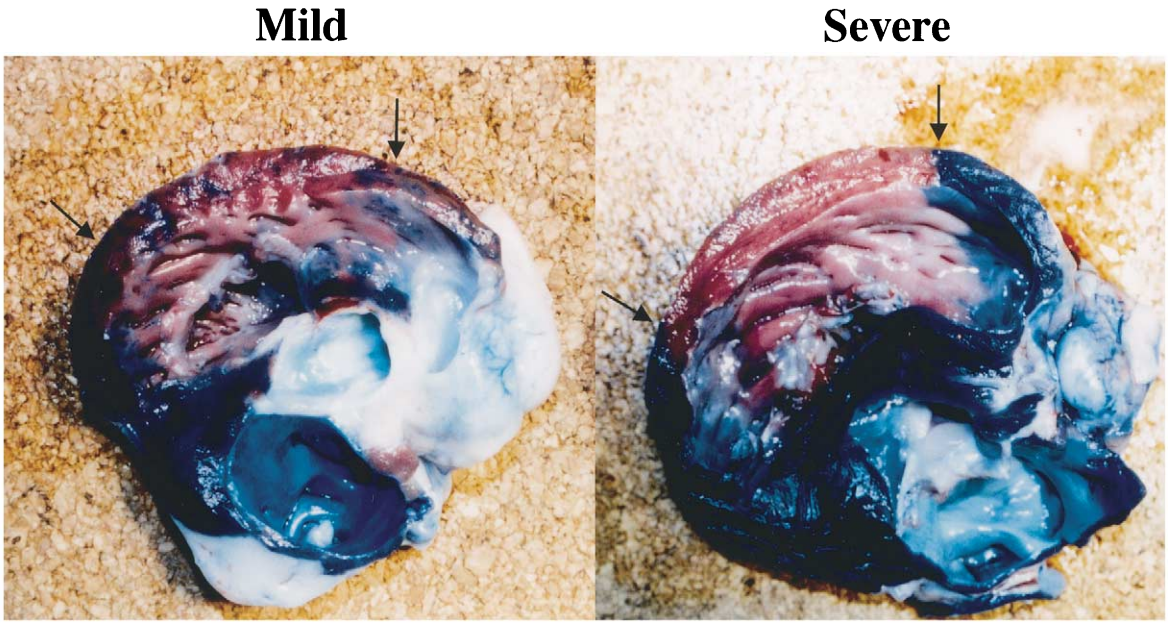

Figure 4. Risk area of the right coronary artery (RCA) delineated by blue dye staining for the slice corresponding to the imaging plane of myocardial contrast echocardiography in the same dogs as in Figures 2 and 3. Regions that were not stained by blue dye **between arrows** denote the RCA bed.

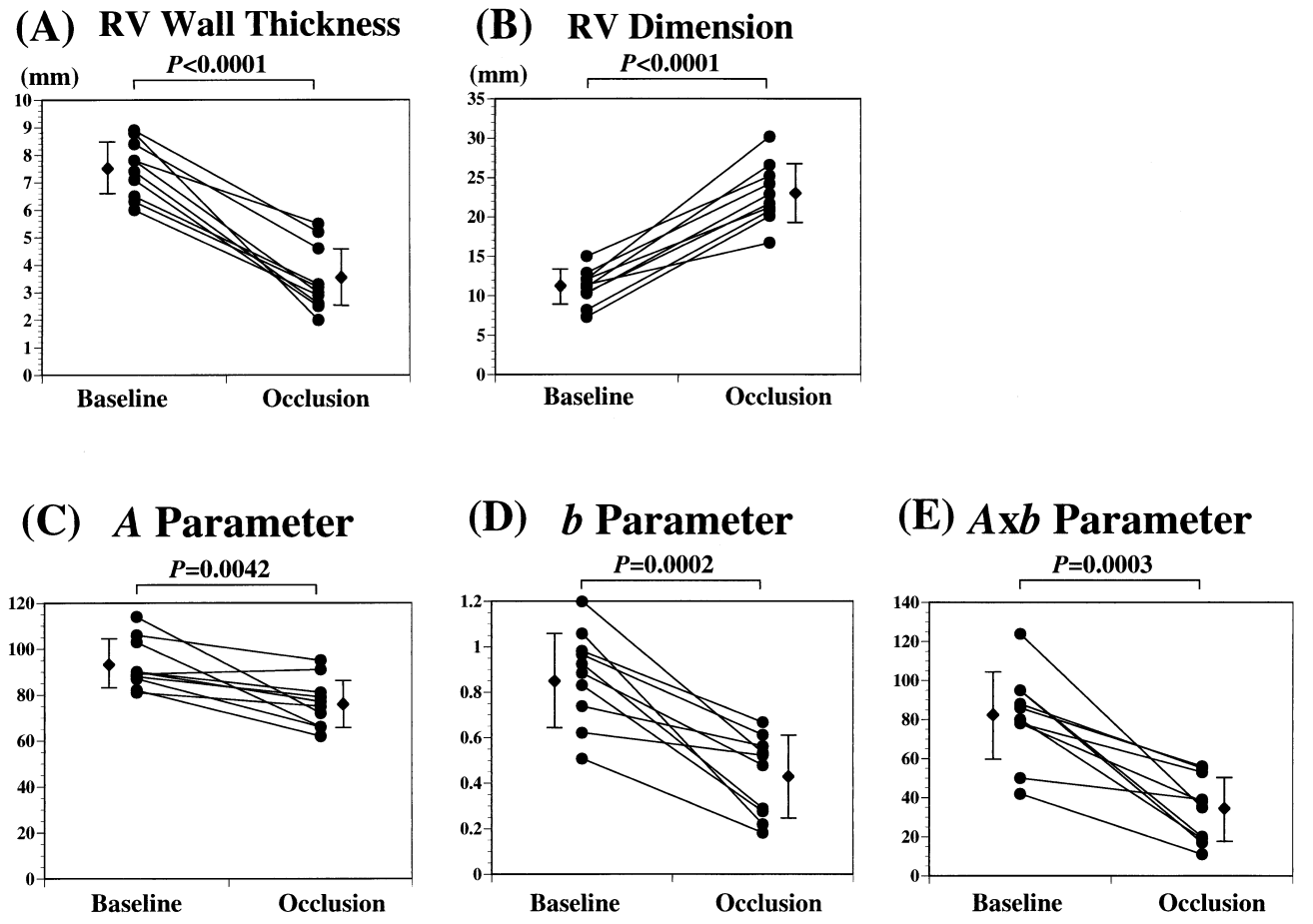

Figure 5. Changes in right ventricular (RV) wall thickness **(A)**, RV dimension **(B)**, and myocardial contrast echocardiography-derived parameters **(C, D, and E)** produced by right coronary artery occlusion.

have clinical implications in assessing abnormal RV myocardial perfusion clinically.

Characteristics of RV opacification defects after RCA occlusion. In the present study, several characteristics of the RV myocardial perfusion abnormalities produced by RCA occlusion on MCE were observed. All dogs in the present study showed patchy opacification defects in the RV wall despite the size of the defect (Fig. 2). The risk area delineated by blue dye also showed heterogeneity of staining similar to that of MCE. Although recent MCE studies (8,9,11) have demonstrated that power Doppler imaging can delineate a transmural perfusion gradient in the LV risk area of left coronary artery (LCA) lesions, the patchy type of opacification defects shown in the present study have not

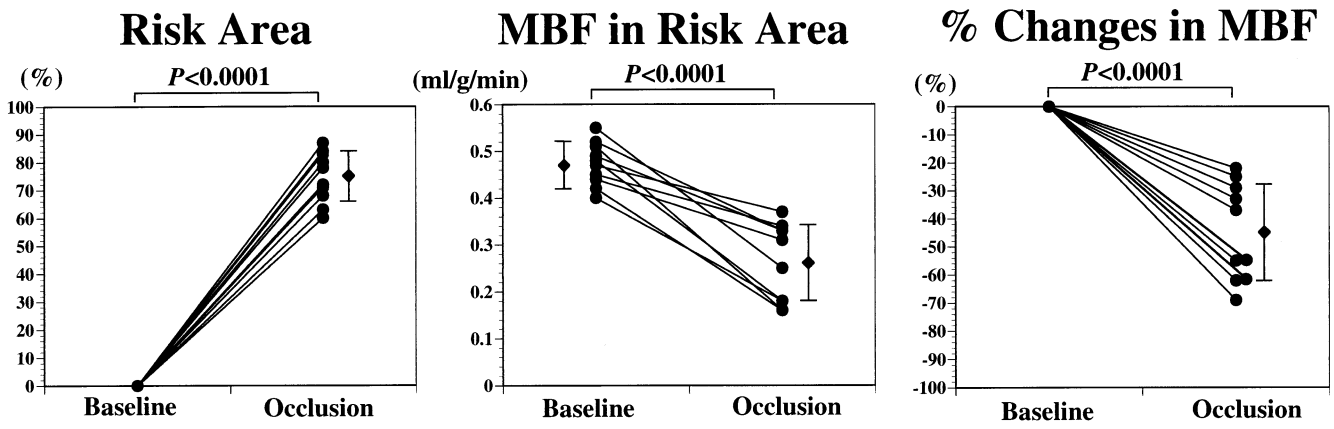

Figure 6. Extent of risk area of an occluded right coronary artery (RCA) delineated by blue dye staining **(left)**, changes in microsphere-derived myocardial blood flow (MBF) in the risk area **(middle)**, and the percent of change in MBF produced by RCA occlusion **(right)**.

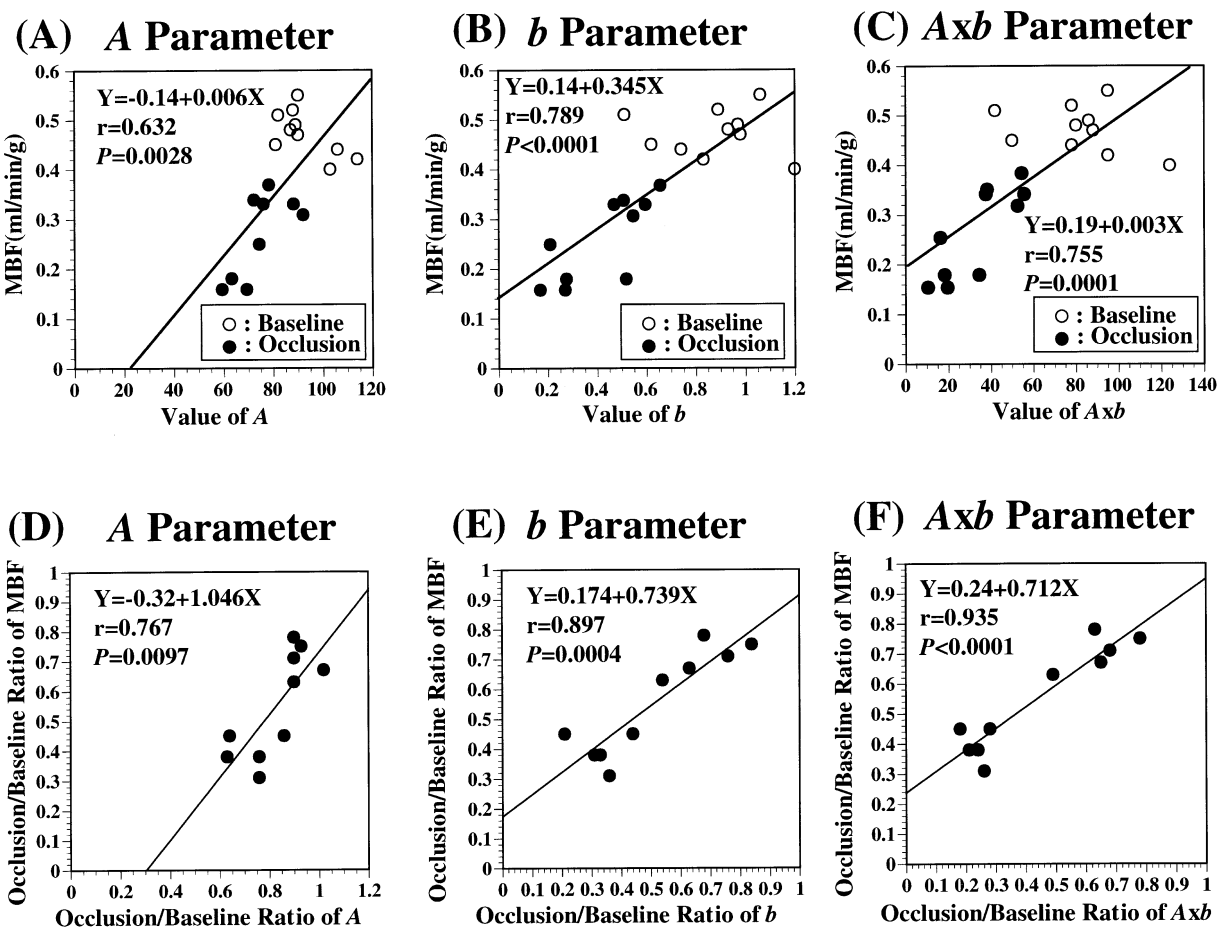

Figure 7. Correlation between myocardial contrast echocardiography-derived parameters (*x*-axis) and microsphere-derived myocardial blood flow (MBF) (*y*-axis).

been reported. In addition, contrast intensity filled in the RV risk area with prolongation of the pulsing interval even during RCA occlusion. This patchy opacification during long pulsing intervals indicates that there is considerable collateral flow from the LCA in this model.

Although the same coronary occlusion was produced at the proximal portion of the RCA in all 10 dogs, changes in microsphere-derived MBF varied considerably. MCE-derived parameters were able to reflect the diverse changes in MBF and correlated well with the MBF in the RCA risk area. As in humans, RCA occlusion did not always produce a similar degree of abnormality in the RV wall in dogs. Laster et al. (12) demonstrated that collateral flow restored RV free wall perfusion to baseline values at seven weeks after RCA occlusion. The data in the present study indicate that severity of RV perfusion abnormalities during acute RCA occlusion depends on collateral flow from the LCA in individual dogs and that MCE can quantify the severity of RV perfusion abnormalities during acute RCA occlusion.

Distinguishing between normal and abnormal RV perfusion. Because it is impossible to compare MCE images before and after RCA occlusion in clinical settings, it is important to assess whether the various parameters (RV wall thickness, RV dimension, and MCE-derived parameters) can differentiate a normal RV perfusion from a state with abnormal perfusion. In the present study, the MCE-derived parameters (*b* and *Axb*) showed greater variation between the baseline period and the RCA occlusion period than did either RV wall thickness or dimension (Fig. 5). In addition, considerable overlap was observed between the baseline and RCA occlusion values for the MCE-derived parameters (*A*, *b*, and *Axb*), but there was little such overlap for either RV wall thickness or dimension. Therefore, measurements of RV wall thickness and dimension may be more useful than MCE-derived parameters for differentiating abnormal RV perfusion from the normal flow state. This limitation of MCE-derived parameters may be attributed to the difficulties in measuring contrast intensity of the thin RV free wall. In the present study, however, there was considerable MBF in the risk area by collateral circulation even when the RCA was occluded (Fig. 6, middle). It may be clinically important to assess residual MBF in the risk area in addition to assessing RV morphological and functional abnormalities. Although changes in RV wall thickness and dimension did not correlate with the decrease in RV MBF produced by RCA occlusion, changes in MCE-derived parameters (*A*, *b*, and *Axb*) correlated well with the decrease in RV MBF in

the risk area. Therefore, MCE-derived parameters are essential for assessing the severity of RV perfusion abnormalities.

Imaging techniques and contrast agent for detecting RV perfusion abnormalities. Levovist has unique features because it is fragile and the microbubble destruction generates a stimulated emission in the presence of high mechanical indices (6,7). For this microbubble, destruction rather than nonlinear microbubble oscillation is likely to result in a great signal intensity that is detected by power Doppler MCE. Thus, we selected a high mechanical index of 1.3 to destroy microbubbles in the present study. In addition, we observed that the location of focus where acoustic power is maximal affected signal intensity in the RV wall in pilot experiments. The signal intensity in the RV wall was less—and was insufficient for the analysis of myocardial perfusion—when the focus was positioned on the LV wall, which was located at the bottom of the imaging field in the pilot experiments. Therefore, the focus was constantly positioned on the RV free wall to obtain maximal signal intensity.

Study limitations. First, when transthoracic imaging is used, the ultrasound pulse will be attenuated to a greater degree than in this open chest study. This may affect the intensity of opacification in the risk area of the RV wall and optimal microbubble dose. Second, we assessed signal intensity from only the RV wall that could be imaged from the narrow echo window. This region was in the central portion of the RV free wall but did not encompass the whole RV free wall. However, tissue examination after euthanizing an animal demonstrated that the risk area was located in the center of the RV free wall and that the extent of the risk area exceeded 60% of the RV free wall in each dog (Fig. 6, left). Thus, the RV wall imaged by MCE in short axis is likely to include the risk area of an occluded RCA. Third, because the coronary circulation differs between dogs and humans, the risk area of an occluded RCA seems to be smaller in the former, as shown both in the present study and a previous report (13). In the present study, the mean value for the risk area expressed as a percentage of the RV short-axis free wall area was 75 ± 9% by blue dye staining (range, 60% to 87%) in this canine model, and the risk area that was not stained by blue dye did not include a part of the RV inferior wall (Fig. 4). Perfusion abnormalities produced by RCA occlusion involve the RV inferior wall, interventricular septum, and LV inferior wall in humans. Perfusion abnormalities of these regions that are in the far field of MCE images may be difficult to visualize, especially by transthoracic MCE in humans. Data obtained from this open chest canine model may be applicable to the assessment of perfusion abnormalities only in the RV anterior wall in clinical settings. Fourth, we selected only the basal segment of the RV free wall for analysis, and thus the mid-ventricular and distal segments were not analyzed. Because we observed few RV perfusion defects and wall motion abnormalities in the mid-ventricular or distal segments in pilot experiments, we selected the basal segment for MCE in the present study. Nonetheless, further studies will be needed to examine which region of the RV free wall is more susceptible to ischemia during RCA occlusion. Finally, we did not create an RCA stenosis in the present study. Diverse levels of RCA stenosis might provide more accurate data regarding the correlation between RV perfusion and wall motion.

Clinical implications. The RV wall is thin, is located beneath the sternum, and exhibits fewer excursions and less thickening than LV myocardium. Detection of RV abnormalities during ischemia or infarction is therefore often difficult. For this reason, the ability to visualize perfusion by MCE may be of considerable value in detecting RV ischemia or infarction. Moreover, the ability to derive refilling parameters may provide a valuable method to quantify the severity of abnormal RV MBF.

Reprint requests and correspondence: Dr. Anthony N. DeMaria, Cardiovascular Division, UCSD Medical Center, 200 West Arbor Street, San Diego, California 92103-8411. E-mail: ademaria@ucsd.edu.

REFERENCES

1. Porter T, Xie F. Transient myocardial contrast after initial exposure to diagnostic ultrasound pressures with minute doses of intravenously injected microbubbles: demonstration and potential mechanism. Circulation 1995;92:2391–5.
2. Kaul S, Senior R, Dittrich H, et al. Detection of coronary artery disease with myocardial contrast echocardiography comparison with 99 mTc-Sestamibi single photon emission computed tomography. Circulation 1997;96:785–92.
3. Wei K, Jayaweera AR, Firoozan S, et al. Quantification of myocardial blood flow with ultrasound-induced destruction of microbubbles administered as a constant venous infusion. Circulation 1998;97:473–83.
4. Zehender M, Kasper W, Kauder E, et al. Right ventricular infarction as an independent predictor of prognosis after acute inferior myocardial infarction. N Engl J Med 1993;328:981–8.
5. Bellamy GR, Rasmussen HH, Nasser FN, et al. Value of two-dimensional echocardiography, and clinical signs in detecting right ventricular infarction. Am Heart J 1986;112:304–9.
6. Agati L, Autore C, Funaro S, et al. Noninvasive assessment of myocardial perfusion: preliminary results in patients with acute myocardial infarction. Am J Cardiol 2000;86:28G–9G.
7. Agati L, Funaro S, Bilotta F. Assessment of no-reflow phenomenon after acute myocardial infarction with harmonic angiography and intravenous pump infusion with Levovist: comparison with intracoronary contrast injection. J Am Soc Echocardiogr 2001;14:773–81.
8. Masugata H, Cotter B, Peters B, et al. Assessment of coronary stenosis severity and transmural perfusion gradient by myocardial contrast echocardiography: comparison of gray-scale B-mode with power Doppler imaging. Circulation 2000;102:1427–33.
9. Masugata H, Lafitte S, Peters B, et al. Comparison of real-time and intermittent triggered myocardial contrast echocardiography for quantification of coronary stenosis severity and transmural perfusion gradient. Circulation 2001;104:1550–6.
10. Glenny RW, Bernard S, Brinkley M. Validation of fluorescent-labeled microspheres for measurement of regional organ perfusion. J Appl Physiol 1993;74:2585–97.
11. Villanueva FS, Gertz EW, Csikari M, et al. Detection of coronary artery stenosis with power Doppler imaging. Circulation 2001;103:2624–30.
12. Laster SB, Shelton TJ, Barzilai B, et al. Determinants of the recovery of right ventricular performance following experimental chronic right coronary artery occlusion. Circulation 1993;88:696–708.
13. de Barros LF, Gutierrez PS. Ligation of the right coronary artery in dogs. Hemodynamic and pathological effects. Arq Bras Cardiol 1991;57:375–9.